Fuel 218 (2018) 366–374

Contents lists available at ScienceDirect

Fuel

journal homepage: www.elsevier.com/locate/fuel

Full Length Article

A novel catalyst CuO-ZrO_2 doped on Cl^- activated bio-char for Hg^0 removal in a broad temperature range

Le Tang[a,b], Caiting Li[a,b,*], Lingkui Zhao[a,b,c], Lei Gao[a,b], Xueyu Du[a,b], Jiawen Zeng[a,b], Jie Zhang[a,b], Guangming Zeng[a,b]

[a] College of Environment Science and Engineering, Hunan University, Changsha 410082, PR China
[b] Key Laboratory of Environmental Biology and Pollution Control (Hunan University), Ministry of Education, Changsha 410082, PR China
[c] College of Environmental Science and Resources, Xiangtan University, Xiangtan 411105, PR China

GRAPHICAL ABSTRACT

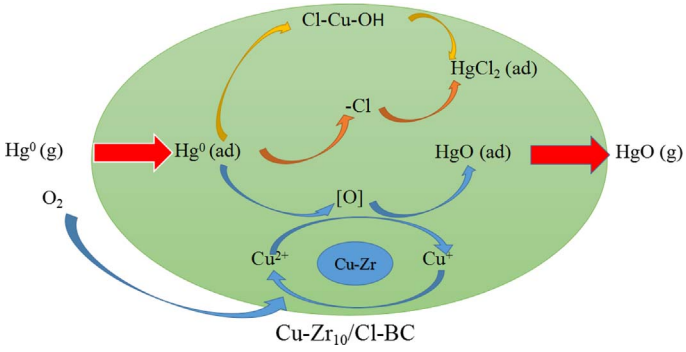

ARTICLE INFO

Keywords:
Bio-char
NH_4Cl
CuO-ZrO_2
Hg^0
Adsorption
Oxidation

ABSTRACT

To obtain a new low-cost catalyst that possesses well Hg^0 removal activity in a broad temperature range, a series of Cu-Zr_x/Cl-BC catalysts were synthesized with the application of bio-char which was activated by NH_4Cl. CuO-ZrO_2 as the active component largely improved Hg^0 removal activity of the catalysts. The catalysts were characterized by SEM-EDX, BET, XRD, H_2-TPR, XPS and FT-IR. When the CuO-ZrO_2 loading value was 10%, Cu-Zr_{10}/Cl-BC reached the best Hg^0 removal efficiency (98.87%) at 120 °C and maintained over 80% until 240 °C. O_2 was of benefit to Hg^0 removal process especially at high temperature because it could regenerate the lattice oxygen which participated in the removal reaction. In addition, Hg^0 removal was mainly determined by adsorption at low temperature and the function of oxidation increased at high temperature. The characterization results indicated that the superior performance of Cu-Zr_{10}/Cl-BC might be ascribed to lower crystallinity, stronger redox ability and better texture properties which resulted from the interaction of CuO and ZrO_2. The mechanism for Hg^0 removal over Cu-Zr_{10}/Cl-BC was also proposed on the basis of above studies.

1. Introduction

As one of air pollutants of coal combustion in coal-fired power plants, elemental mercury (Hg^0) has attracted a great deal of concern due to its toxicity, volatility and bio-accumulation [1,2]. It is hard to remove cleanly and will leave bad effects on both human and the environment [3]. The US Environmental Protection Agency issued the national standard Final Mercury and Air Toxic Standards for the control

* Corresponding author at: College of Environment Science and Engineering, Hunan University, Changsha 410082, PR China.
E-mail address: ctli@hnu.edu.cn (C. Li).

https://doi.org/10.1016/j.fuel.2018.01.051
Received 31 October 2017; Received in revised form 5 January 2018; Accepted 13 January 2018

of mercury, acid gases and other harmful air contaminants on April, 19, 2012 [4]. Mercury and its compounds were limited to 0.03 mg/m^3 by the Ministry of Environmental Protection of China (MEPC) [5]. Therefore, a series of measures have been taken to investigate and handle Hg^0 emission issues.

Up to now, many methods have been studied to remove Hg^0 in the flue gas. Wet flue gas desulfurization (WFGD) is regarded as a good method for the SO_2 removal, it also be used to remove Hg^{2+} after the oxidation of Hg^0 in the industry. But, the re-emission of mercury during the WFGD is a serious problem [6]. Activated carbon injection (ACI) has been recognized as the mainly commercialized technology to dispose Hg^0 at the temperature window of 100–200 °C [7], and activated carbons modified by sulfur, chloride and metal oxide (CuO, MnO_2, V_2O_5) were widely used [8,9]. However, the main problems related to ACI include the large consumption and low utilization rate, which might increase the cost immensely [10]. Therefore, it is important to develop a new material with low cost and high activity to replace the commercial activated carbon. Bio-char (denoted as BC below) has received considerable attention for Hg^0 removal due to its characteristics of going green, environmental protection and low-cost [11,12]. It could be obtained by pyrolysis of various biomass which are from cheaper source, including bamboo, corn cob, sawdust and so on [5]. It is well known that pine nut has become popular among Chinese family as one of the nut food. In order to improve economics of the material, pine nut shell might be suitable and cheap source for BC as the raw material for Hg^0 removal. However, the original pyrolysis products of bio-char were not effective enough for Hg^0 removal [13]. Hence, how to enhance the Hg^0 removal efficiency of bio-char is becoming popular. Recently, the literature reported that impregnated Cl element could greatly help activated carbon adsorbing Hg^0 in the flue gas [14]. For example, Li et al. [15] have indicated that the bio-char (prepared by both microwave and 5 wt% NH_4Cl loading) was a cost-effective Hg^0-capture sorbent. Tan et al. [16] have suggested that $ZnCl_2$ modified bamboo charcoals had excellent adsorption activity of elemental mercury. Nevertheless, new problem came out that the efficient temperature of halogen activated bio-char often existed at lower temperature window (60–100 °C) [15,17]. Therefore, developing a novel low cost catalyst which not only possess excellent Hg^0 removal efficiency at low temperature but also can maintain well activity at higher temperature is desirable.

It is worth noting that CuO has been demonstrated to have high oxidation activity for NO_x and SO_x [18]. In addition, many types of doped Cu based catalysts with excellent Hg^0 removal catalytic activity have also been investigated [19,20]. For instance, Wang et al. [21] have studied the oxidation of Hg^0 by CuO-MnO_2-Fe_2O_3/γ-Al_2O_3, which indicated that the active Cu^{2+} phase participated in the reaction and be reduced to Cu^+. Cu^{2+} could enhance SCR performance and mercury removal efficiency over CeO_2-CuO catalyst [22]. Interestingly, most of researches have been focusing on the effect of ZrO_2 combined with another metal oxide for mercury removal. The reason was that ZrO_2 additive could essentially benefit the catalysts performance with high temperature durability [23]. Li et al. [24] have deduced that the synergetic effect between Ce and Zr might result in the high Hg^0 catalytic oxidation efficiency of CeO_2(ZrO_2)/TiO_2. Xie et al. [25] developed a novel regenerable sorbent based on Zr-Mn binary metal oxides, and proved that Zr significantly improved the sorbent's mercury removal capacity at 75–200 °C. Unfortunately, comparatively fewer investigations of CuO-ZrO_2 doped on Cl^- activated bio-char for Hg^0 removal have been reported.

Herein, the purpose of this study was to investigate the performance and mechanism of CuO-ZrO_2 doped on Cl^- activated bio-char for Hg^0 removal in simulated flue gas at 60–270 °C, and the effect of CuO-ZrO_2 doped on Hg^0 removal was evaluated. The role of flue gas components (O_2, NH_3, SO_2, H_2O) in the Hg^0 removal was also examined. Besides, SEM-EDX, BET, XRD, H_2-TPR, XPS and FTIR were used to characterize the physicochemical properties of catalysts and to discuss the reaction mechanism.

2. Materials and methods

2.1. Preparation of catalysts

10 g pine nut shell used as the original material was crushed and sieved to 80–100 mesh, and became about 4 g BC after calcination in an electric tube furnace at 600 °C for 2 h under N_2 atmosphere. Then, the requisite amount of NH_4Cl was dissolved in deionized water with 1 h vigorous stirring to form 5% (mass fraction) NH_4Cl solution. A certain amount of BC (BC/NH_4Cl solution = 1 g:20 ml) was added to the solution with vigorous stirring for 4 h, after aging for 12 h, the mixture was dried in an electric blast drying oven at 90 °C for 24 h. The obtained NH_4Cl-biochar support was denoted as Cl-BC.

A series of catalysts were synthesized using impregnation method. The molar ratio of CuO and ZrO_2 was set as 1:1. Typically, 0.286 g Cu$(NO_3)_2{\cdot}3H_2O$ and 0.382 g $ZrOCl_2{\cdot}8H_2O$ were dissolved in 10 ml deionized water (support/deionized water = 1 g:5 ml). After stirring 1 h, the mixed solution was impregnated on 2 g Cl-BC support and stirred for 4 h. Subsequently, the mixture was aged for another 12 h. Then, the mixture was dried in an electric blast drying oven at 105 °C for 24 h and finally calcined in an electric tube furnace at 450 °C for 4 h at a heating rate of 5 °C/min under N_2 atmosphere. The obtained catalyst was denoted as Cu-Zr_{12}/Cl-BC, and another Cu-Zr_x/Cl-BC materials were also prepared by the same steps with different consumption of Cu$(NO_3)_2{\cdot}3H_2O$ and $ZrOCl_2{\cdot}8H_2O$ (where x represented the mass percentage of CuO-ZrO_2 to Cl-BC (x = 2, 4, 6, 8, 10, 12), Cu represented CuO and Zr symbolized ZrO_2).

Besides, to understand the effect of each element on mercury removal, Cu-Zr/BC, Cu/Cl-BC and Zr/Cl-BC were prepared with the same processes which have the corresponding element blank.

2.2. Characterization of catalysts

The catalyst microstructure and morphology were observed by scanning electron microscopy (SEM) (Quanta FEG 250, USA). Every image of catalysts was magnified to 10,000×. Energy Dispersive X-ray Analysis (EDX) was used to analyze the elementary composition of each catalyst.

Micromeritics Tristar II 3020 analyzer (Micromeritics Instrument Crop, USA) was used to analyze the Brunauer-Emmett-Teller (BET) surface area, pore volume and average pore diameter of catalysts from N_2 adsorption isotherm.

The X-ray diffraction was used to determine the crystalline phases of catalysts, which carried out on a Rigaku D/Max 2500 (Rigaku Corporation, JPN). And the patterns were obtained in the 2θ range from 10 to 80° with Cu Kα radiation.

The Temperature-programmed reduction of H_2 (H_2-TPR) was measured on TP-5080 automated chemisorption analyzer (Xian quan Tianjing China).

X-ray photoelectron spectroscopy was measured by a K-Alpha 1063 system (Thermo Fisher Scientific, UK) with an Al Kα X-ray source. The binding energy was corrected by C1s at 284.6 eV.

The Fourier Transform Infrared Spectroscopy (FT-IR) was conducted on IRAffinity-1 (Shimadzu, Japan). Prior to each test, every sample was treated at 250 °C under pure N_2 for 1 h to remove adsorbed species on the surface and cooled to room temperature. The FT-IR experiments were conducted immediately after each reaction, and the reaction conditions were as follows: $NH_3 + O_2$ (500 ppm NH_3, 6% O_2/N_2), $SO_2 + O_2$ (400 ppm SO_2, 6% O_2/N_2), $NH_3 + NO + O_2$ (500 ppm NH_3 + 500 ppm NO, 6% O_2/N_2), $H_2O + O_2$ (8 vol% H_2O, 6% O_2/N_2). The total gas flow was 500 ml/min.

2.3. Test of catalytic performance

The experimental setup for evaluating the Hg^0 removal is shown in Fig. S1. Cu-Zr_x/Cl-BC catalysts were tested in a fixed bed continuous

flow quartz reactor (i.d. 10 mm) at atmospheric pressure. 0.1 g catalyst was placed in quartz tube and a digital temperature controller regulated the reaction temperature from 60 to 270 °C. The simulated flue gas contained 90.0 ug/m^3 Hg^0, 6% O_2 and balance N_2 (99.99%). 500 ppm NO, 500 ppm NH_3, 400 ppm SO_2, 8 vol% H_2O would be added when used. The total flow rate was 500 ml/min (GHSV = about 20,0000 h^{-1}) and controlled by mass flow controllers accurately. Gas-phase Hg^0 was generated by a Hg^0 permeation tube (VICI Metronics, USA) and carried by 200 ml/min high purity N_2 (99.999%).

The inlet and outlet concentrations of Hg^0 were measured by an online RA-915M mercury analyzer (LUMEX Ltd, Russia), and its detection limitation is 0.001 ug/m^3. To identify the concentration of total mercury (Hg^T), oxidized mercury (Hg^{2+}) and elemental mercury (Hg^0) at the reactor outlet, a mercury speciation conversion system (a gas washing bottle containing a 10% $SnCl_2$ aqueous solution or 10% KCl aqueous solution) was set in front of the mercury analyzer. The gas passed through $SnCl_2$ solution to reduce the Hg^{2+} into Hg^0 and the Hg^T could be measured. When the gas passed through KCl solution, Hg^{2+} would be captured and content of Hg^0 could be measured. The concentration of Hg^{2+} could be calculated by the difference between Hg^T and Hg^0. The total Hg^0 removal efficiency (E_T), the Hg^0 oxidation efficiency (E_{oxi}) and the Hg^0 adsorption efficiency (E_{ads}) could be defined as Eqs. (1-3):

$$E_T = \frac{Hg^0_{in} - Hg^0_{out}}{Hg^0_{in}} \times 100\% \quad (1)$$

$$E_{oxi} = \frac{Hg^T_{out} - Hg^0_{out}}{Hg^0_{in}} \times 100\% \quad (2)$$

$$E_{ads} = \frac{Hg^0_{in} - Hg^T_{out}}{Hg^0_{in}} \times 100\% \quad (3)$$

In which Hg^0_{in} and Hg^0_{out} denote the inlet Hg^0 concentration and outlet Hg^0 concentration (ug/m^3) respectively, Hg^T_{out} denote the outlet Hg^T concentration (ug/m^3. comment: all data below were obtained from the average of three experimental results).

3. Results and discussion

3.1. Property of Hg^0 removal

3.1.1. Effect of -Cl and CuO-ZrO_2 into Cu-Zr_x/Cl-BC on Hg^0 removal

The comparison of catalytic performance on Hg^0 removal over different catalysts at a series of temperature from 60 to 270 °C is shown in Fig. 1 (a). It was obvious that the E_T of BC support was very low. However, the E_T of Cl-BC support was improved at low temperature compared to BC. The main reason might be that the Cl^- on the surface of the samples enhanced the Hg^0 adsorption capacity [26]. Interestingly, the activity of CuO-ZrO_2 loaded catalysts was significantly higher than the one loaded with pure CuO or pure ZrO_2. After the addition of CuO-ZrO_2 mixed oxides, E_T of the catalysts greatly increased over the whole temperature range, which suggested that CuO-ZrO_2 mixed oxides played a significant role in Hg^0 removal reaction. It could be seen that Cu-Zr_6/Cl-BC exhibited the best E_T (95.02%) at 120 °C. In addition, E_T of Cu-Zr_6/Cl-BC and Cu-Zr_6/BC were above 80% from 90 to 180 °C and could remain over 60% until 210 °C. However, Cl-BC support showed good removal efficiency at first, and then dropped rapidly as the temperature increased. It could be concluded that the addition of CuO-ZrO_2 mixed oxides widened the temperature window of the reaction as well as considerably promoted catalytic performance.

3.1.2. Effect of Cu-Zr loading value on Hg^0 removal

To investigate more about the effect of CuO-ZrO_2 doped on Hg^0 removal, relevant experiments were conducted, and the results are shown in Fig. 1 (b). It was clearly found that the catalytic activity was affected by the Cu-Zr loading value. Cu-Zr_{10}/Cl-BC showed the best performance (98.87%) on Hg^0 removal at 120 °C, Cu-Zr_8/Cl-BC and Cu-Zr_{12}/Cl-BC also exhibited good activity in the entire range of temperature. It could be seen that removal efficiency improved as the loading value increased to 10%, and decreased a bit when loading value was 12% in the whole temperature range. What deserved to be mentioned was that the higher Cu-Zr loading value the catalysts owned, the stronger resistance to high temperature the samples possessed. It was said that the Hg^0 removal activity mainly depended on absorption effect at low temperature while catalytic oxidation would become apparent during the process at high temperature [27]. Hence, it could be deduced that CuO-ZrO_2 could in favor of Hg^0 oxidation. In the whole reaction temperature range, the optimal value for the mass percentage of CuO-ZrO_2 was 10%. Therefore, Cu-Zr_{10}/Cl-BC was used in latter experiments.

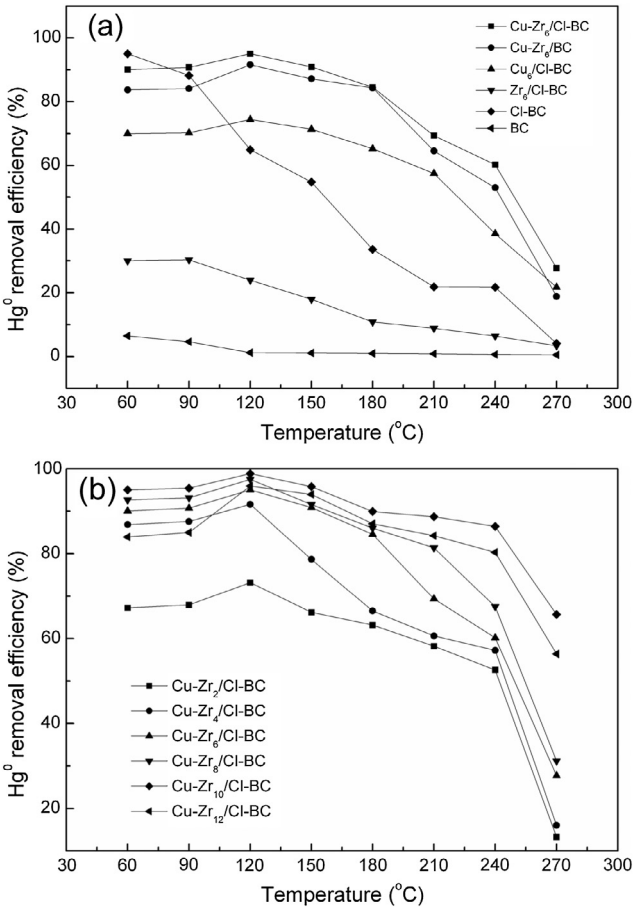

Fig. 1. (a) Hg^0 removal over different catalysts; (b) Effect of loading value on removal of Hg^0 over Cu-Zr_x/Cl-BC. Reaction condition: 60–270 °C, 0.1 g of catalyst, Hg^0 = 90 ug/m^3, O_2 = 6%, balanced N_2.

3.1.3. Experiment of mercury conversion

Understanding the mercury speciation transformation could help us to learn the mechanism of the reaction between catalysts and Hg^0. The mercury conversion experiment was taken and the results are shown in Fig. 2. Experimental sample was Cu-Zr_{10}/Cl-BC and reaction temperature was set as 120 °C. With the time passed, E_T still maintained a high level at the first 2 h, and then decreased gradually and kept stable at last, the same as the E_{ads} of Cu-Zr_{10}/Cl-BC. It could be seen that the E_{oxi} was 9.32% at first and reached 30.15% eventually. It was speculated that an amount of oxidized mercury would form at high temperature. Moreover, the result further proved that the catalyst has a certain oxidation activity during Hg^0 removal process.

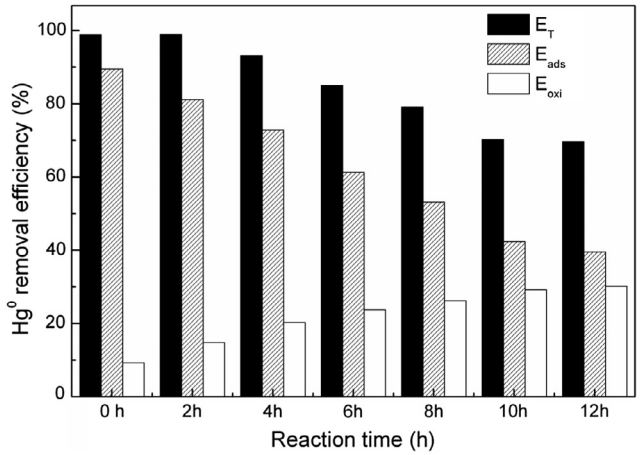

Fig. 2. Mercury conversion experiment over Cu-Zr_{10}/Cl-BC. Reaction condition: 120 °C, 0.1 g of catalyst, Hg^0 = 90 ug/m^3, O_2 = 6%, balanced N_2.

3.2. Effect of O_2 and NH_3

To further study the adsorption and catalytic oxidation of Hg^0, the experiments about the influence of different O_2 concentration over Cu_{10}/Cl-BC and Cu-Zr_{10}/Cl-BC at 120, 240 °C (compared at low and high temperatures) were conducted. As shown in Fig. 3, in the absence of O_2, E_T of Cu_{10}/Cl-BC and Cu-Zr_{10}/Cl-BC at 120 °C were superior to that at 240 °C. It could be deduced that adsorption played a key role in this removal process without O_2. For Cu-Zr_{10}/Cl-BC, when O_2 added to 3%, the advance of E_T was not apparent, and no significant change happened when the O_2 content increased from 3% to 12% at 120 °C. While at 240 °C, the E_T enhanced more than 60% when added 3% O_2, and kept improving as O_2 content increased, which illustrated that O_2 had an obvious effect on Hg^0 removal at 240 °C. According to some researches [27,28], it was said that Hg^0 removal primarily depends on the adsorption at low temperature, while the effect of adsorption would decrease and oxidation effect increase at high temperature. Therefore, it could be concluded that Hg^0 removal mainly determined by the adsorption at low temperature, and the catalytic oxidation just occupied a bit part, 3% O_2 was sufficient for enhancement of E_T. Catalytic oxidation became apparent at high temperature. Compared to Cu_{10}/Cl-BC, the E_T of Cu-Zr_{10}/Cl-BC was much better, which was consistent with the results of Fig. 1. Besides, the increased amount of E_T over Cu-Zr_{10}/Cl-BC was far beyond Cu_{10}/Cl-BC when O_2 increased from 0 to 3% at 240 °C. According to the results of later XPS discussions, it could be inferred that lattice oxygen participated in Hg^0 oxidation. That was Hg^0 reacted with lattice oxygen to form HgO on the surface of Cu-Zr_{10}/Cl-BC. It also could be speculated that the addition of Zr improved oxygen storage capacity of the materials and promoted the effect of oxidation.

Many researches [28,29] indicated that NH_3 exhibited prohibitive impact on Hg^0 adsorption and oxidation. To deeper discuss the role of adsorption and oxidation in this study, the effect of NH_3 was investigated and the results are presented in Fig. 4 (a). After 500 ppm NH_3 being added at 2 h, the E_T decreased by 9.88% at 120 °C, while it decreased by 19.35% at 240 °C after 10 h. The inhibition of NH_3 primarily

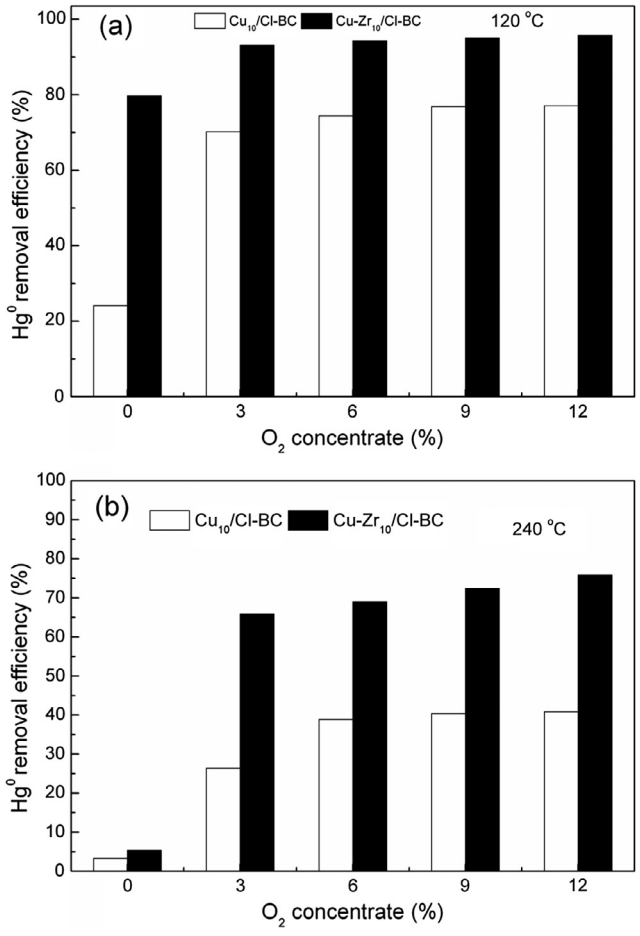

Fig. 3. Effect of O_2 on removal of Hg^0 over Cu_{10}/Cl-BC and Cu-Zr_{10}/Cl-BC. Reaction condition: 0.1 g catalyst, Hg^0 = 90 ug/m^3, O_2 = 0–12%, balanced N_2 (a) 120 °C (b) 240 °C.

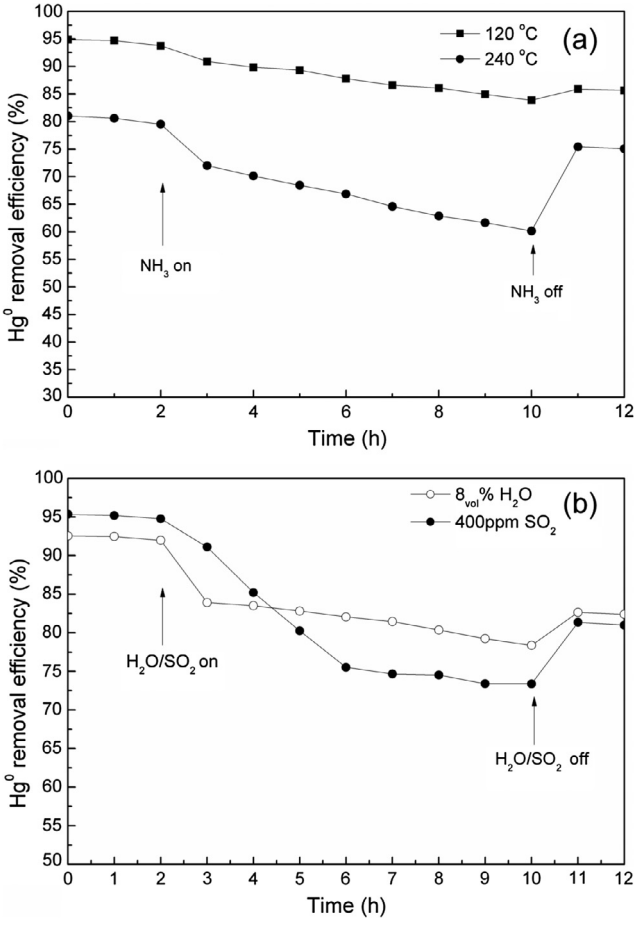

Fig. 4. Effect of NH_3, H_2O and SO_2 on removal of Hg^0 over Cu-Zr_{10}/Cl-BC. Reaction condition: 0.1 g of catalyst, Hg^0 = 90 ug/m^3, O_2 = 6%, balanced N_2. (a) NO = 500 ppm, NH_3 = 500 ppm (when used) (b) NH_3 = NO = 500 ppm, H_2O = 8 vol% (when used), SO_2 = 400 ppm (when used).

showed as the decrease of adsorption at low temperature, which was due to the competitive adsorption between Hg^0 and NH_3 [30]. The inhibition mainly showed as the decline of Hg^0 oxidation at high temperature because NH_3 could react with the catalyst to generate adsorbed species such as adsorbed NH_3 and NH_4^+ that could occupy the active sites and consume surface active oxygen [28]. The results were corresponding to the analysis of the spectra of NH_3+O_2 adsorption in Fig. 9 (b). After 10 h, the Hg^0 removal activity recovered immediately by cutting off NH_3. Combined with the effect analysis of O_2 and NH_3 above, it could be deduced that Hg^0 removal was mainly determined by adsorption at low temperature and oxidation effect became obvious at high temperature.

3.3. Resistance ability to H_2O and SO_2

Since the effect of SO_2 and H_2O are prominent for Hg^0 removal in practical applications, the experiments about the influence of SO_2 and H_2O over Cu-Zr_{10}/Cl-BC were conducted. As shown in Fig. 4 (b), when 8 vol% H_2O and 400 ppm SO_2 were introduced, E_T decreased to approximately 78.3% and 73.3% respectively after 10 h. However, it was still at high level of catalytic activity for Hg^0 removal. It could be illustrated that the Cu-Zr_{10}/Cl-BC catalyst presented well resistance to H_2O and SO_2. When cutting off the H_2O and SO_2, the Hg^0 removal efficiency gradually recovered but not returned to the original level yet. It implied that the catalysts were deactivated by H_2O and SO_2. The possible reason was that water competed with mercury for the active adsorption sites [31]. Nevertheless, the activation of NH_4Cl on bio-char provided more adsorption sites such as –Cl which could weaken the deactivation of H_2O. The deactivation of SO_2 for Hg^0 removal might also owing to the competitive adsorption between SO_2 and Hg^0 on the surface of Cu-Zr_{10}/Cl-BC catalyst [32]. Combined with the analysis above, it could be demonstrated that the Cu-Zr_{10}/Cl-BC catalyst possessed well H_2O and SO_2 resistance, which was in favor of the practical application on Hg^0 removal from flue gas.

3.4. Stability test of the catalyst

The stability test for Hg^0 removal over Cu-Zr_{10}/Cl-BC was performed at 120 °C for 32 h, the detailed description is listed in Supplementary material and the result is shown in Fig. S2.

3.5. Characterization results

3.5.1. SEM - EDX analysis

The texture and morphology properties of catalysts were investigated by SEM, and the images are shown in Fig. 5(a)–(f). As seen in Fig. 5(a), the micro particles of BC were agglutination. Compared to BC, there were many pores formed on the surface of Cl-BC, indicating that the ability of adsorption would be enhanced, and this phenomenon was consistent with the result of Hg^0 removal ability in Fig. 1(a). After the addition of CuO, it could be seen that there existed white solid on the surface of Cu_6/Cl-BC. It may be the crystal of copper oxide species. While, with the addition of ZrO_2, the white solid disappeared, suggesting that the interaction between CuO and ZrO_2, which made the active components well dispersed on the surface of Cu-Zr_x/Cl-BC. According to the average pore diameter from BET analysis, the most pores on the catalysts were micropore. Compared to Cu-Zr_6/Cl-BC, the surface of Cu-Zr_{10}/Cl-BC became smoother and the micropore distributed more homogeneously which was also consistent with superior E_T. To determine the contents of CuO and ZrO_2, ICP-OES analysis were performed. The detailed description is listed in Supplementary material and the result is shown in Table S1.

The results of the SEM-EDX analysis are shown in Table 1, the contents of these elements were little lower than the caculated contents, which was probably because that SEM-EDX just determined the surface composition and layer morphology of the catalysts. C was the most abundant element on the surface, and the content of O increased with the increasing metal loading. The content of Cl (2.71 wt%) on Cu-Zr_{10}/Cl-BC was the most, suggesting that Cl might participated in Hg^0 removal process. It was said that Cl could react with C to form C–Cl groups [15]. What to be sure was that the main active components were loaded on the bio-char surface successfully.

3.5.2. BET

The BET specific surface area, pore volume and average pore diameter of catalysts are presented in Table 2. Compared to BC, the surface area, pore volume and average pore diameter of Cl-BC increased obviously, which was attributed to many new pores formed on the surface of Cl-BC, and it was in accordance with the images of SEM. After loading of metal oxides, the average pore diameter changed a little, the BET surface area and pore volume increased, and Cu-Zr_{10}/Cl-BC

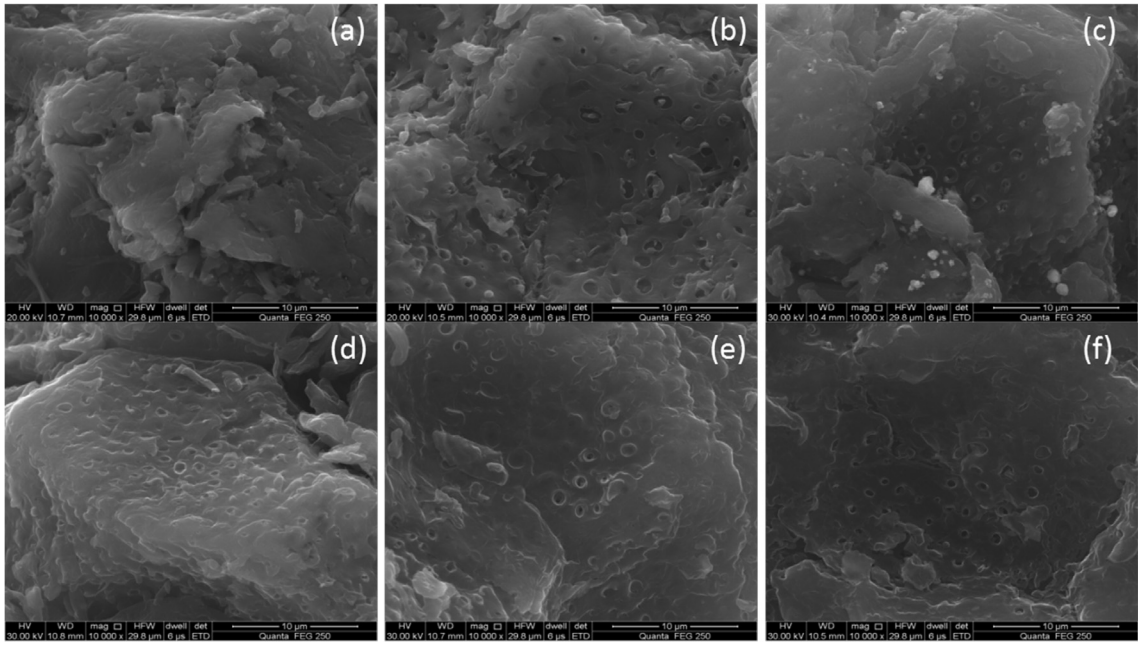

Fig. 5. SEM photographs of (a) BC, (b) Cl-BC, (c) Cu_6/Cl-BC, (d) Cu-Zr_6/BC, (e) Cu-Zr_6/Cl-BC, (f) Cu-Zr_{10}/Cl-BC, magnification: 10,000×.

Table 1
Content of five main elements defined by EDX. (Unit: wt%).

Sample	C	O	Cl	Cu	Zr
Zr_6/Cl-BC	95.61	1.88	0.57	0	1.94
Cu_6/Cl-BC	93.14	2.36	0.31	4.19	0
Cu-Zr_6/BC	92.62	2.78	0.07	2.09	2.44
Cu-Zr_6/Cl-BC	90.01	3.07	1.65	2.76	2.51
Cu-Zr_{10}/Cl-BC	81.8	4.53	2.71	4.4	6.56

displayed the most large surface area (340.8 m^2/g) and pore volume (0.159 cm^3/g). With the results of SEM and BET, it could be deduced that the cooperation of CuO and ZrO_2 not only facilitated the well dispersion of metal oxide species and large surface area but also promoted the texture properties, which contributed to the excellent catalytic activity for Hg^0 removal.

3.5.3. XRD

As presented in Fig. 6, XRD measurements were conducted to study the crystal structure of different catalysts. For Cu_6/Cl-BC, the peaks at 35.5°, 38.6° related to the lattice plane of (1 1 1) were corresponding to well crystallized CuO phase (PDF-ICDD 80-1916, 80-0076) [33,34]. The peaks at 36.5°, 61.4° related to the lattice planes of (1 1 1), (2 2 0) respectively were attributed to Cu_2O phase (PDF-ICDD 78-2076) [34]. For Zr_6/Cl-BC, the peaks at 30.2°, 35.1°, 50.3°, 60.0° related to the lattice planes of (1 0 1), (1 1 0), (1 1 2), (2 1 1) respectively were attributed to ZrO_2 (PDF-ICDD 81-1544) [18]. When ZrO_2 was added in, the peaks ascribed to copper oxide disappeared, which was probably due to the well dispersion or amorphous structure on the surface of Cl-BC support. Results indicated that the addition of ZrO_2 could weaken the crystallinity, or maybe there existed interaction between CuO and ZrO_2. The peaks at 16.1°, 32.4°, 39.4° were the crystals formed by Cu, Cl, O, H, which were related to $Cu_2Cl(OH)_3$ (PDF-ICDD 78-0372). It was worth mentioning that the height of half-peak breadth of $Cu_2Cl(OH)_3$ increased as the loading value increased, and it was highest on Cu-Zr_{10}/Cl-BC. Besides, a small peak at 39.8° was ascribed to $Cu(OH)_2$ (PDF-ICDD 80-0656) which might come from the decomposition of part $Cu_2Cl(OH)_3$.

3.5.4. H_2-TPR

The results of H_2-TPR investigation are shown in Fig. 7, the reducibility of Cu_6/Cl-BC, Zr_6/Cl-BC, Cu-Zr_6/Cl-BC, and Cu-Zr_{10}/Cl-BC were studied. The reduction peaks at 225 °C, 334 °C, 287 °C of Cu_6/Cl-BC, Cu-Zr_6/Cl-BC, Cu-Zr_{10}/Cl-BC respectively were assigned to the reduction of dispersed copper oxide [13,19], and the peaks centered at 380 °C, 433 °C, 402 °C of three catalysts respectively were correspond to reduction of CuO species as a bulk form [35]. There existed no peaks related to ZrO_2 of Zr_6/Cl-BC, because pure ZrO_2 showed little reduction peak when the temperature below 900 °C [36]. As the ZrO_2 added into the catalyst, two peaks of Cu-Zr_6/Cl-BC shifted to high temperature compared to Cu_6/Cl-BC, this phenomenon was similar to the result of Wang et al. [18] and Liu et al. [37]. When the loading value increased to 10%, the two peaks shifted to lower temperature in comparison with Cu-Zr_6/Cl-BC, indicating that Cu-Zr_{10}/Cl-BC had better redox ability. Meanwhile, it was notable that the peak area increased in the order of

Table 2
The surface area, pore volume and average pore diameter of catalysts.

Sample	BET surface area (m^2/g)	Pore volume (cm^3/g)	Average pore diameter (nm)
BC	131.517	0.049	1.573
Cl-BC	206.664	0.101	1.952
Zr_{10}/Cl-BC	220.293	0.102	1.858
Cu_{10}/Cl-BC	328.004	0.152	1.852
Cu-Zr_{10}/Cl-BC	340.825	0.159	1.872

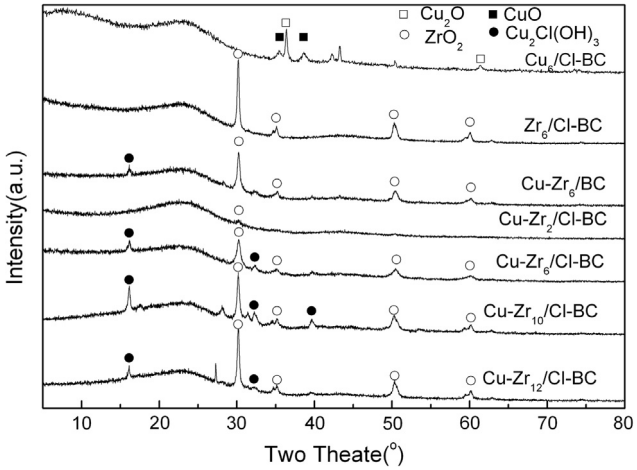

Fig. 6. XRD patterns of Cu_6/Cl-BC, Zr_6/Cl-BC, Cu-Zr_6/BC, Cu-Zr_2/Cl-BC, Cu-Zr_6/Cl-BC, Cu-Zr_{10}/Cl-BC, Cu-Zr_{12}/Cl-BC.

Cu_6/Cl-BC, Cu-Zr_6/Cl-BC, Cu-Zr_{10}/Cl-BC, hence, the reducibility improved as the same order. Higher redox ability could enhance the mobility of surface oxygen and improve the E_T, which in accord with the results of Fig. 1.

3.5.5. XPS

To gain more insight into Hg^0 removal mechanisms and identify the chemical state of elements on the surface of catalysts, the XPS analysis was conducted on fresh Cu_{10}/Cl-BC, Zr_{10}/Cl-BC, Cu-Zr_{10}/Cl-BC and used Cu-Zr_{10}/Cl-BC. As shown in Fig. 8 (a), the O 1s spectrum was divided into three main peaks, the first peak at around 530.2–530.5 eV could be assigned to the lattice oxygen O^{2-} (denoted as O_β), the second peak at around 531.7 eV was attributed to chemisorbed oxygen (denoted as O_α), and the third peak at higher banding energy corresponded to hydroxyl species and/or adsorbed water species (denoted as O_γ) [33,38]. The ratio of O_β/O_T ($O_T = O_\beta + O_\alpha + O_\gamma$) of fresh Cu-$Zr_{10}$/Cl-BC (33.5%) was higher than that of fresh Cu_{10}/Cl-BC (26.2%) and Zr_{10}/Cl-BC (12.4%), which indicated that the amount of lattice oxygen species on Cu-Zr_{10}/Cl-BC catalyst was increased. Compared to fresh Cu-Zr_{10}/Cl-BC, the ratio of O_β/O_T decreased from 33.5% to 23.5% and O_γ/O_T decreased from 44.9% to 39.3% over used Cu-Zr_{10}/Cl-BC, which demonstrated that both hydroxyl oxygen (OH) and lattice oxygen participated in Hg^0 oxidation [27]. The increase of chemisorbed oxygen might result from the compensation of O_2.

The Cu 2p spectra is shown in Fig. 8(b). It has been reported that the higher Cu $2p_{3/2}$ band at 934.4–935.8 eV, the shake-up peak at around

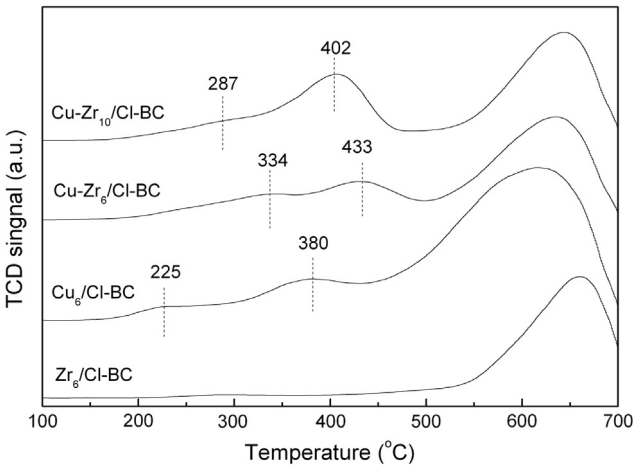

Fig. 7. H_2-TPR profiles for Cu_6/Cl-BC, Zr_6/Cl-BC, Cu-Zr_6/Cl-BC, Cu-Zr_{10}/Cl-BC.

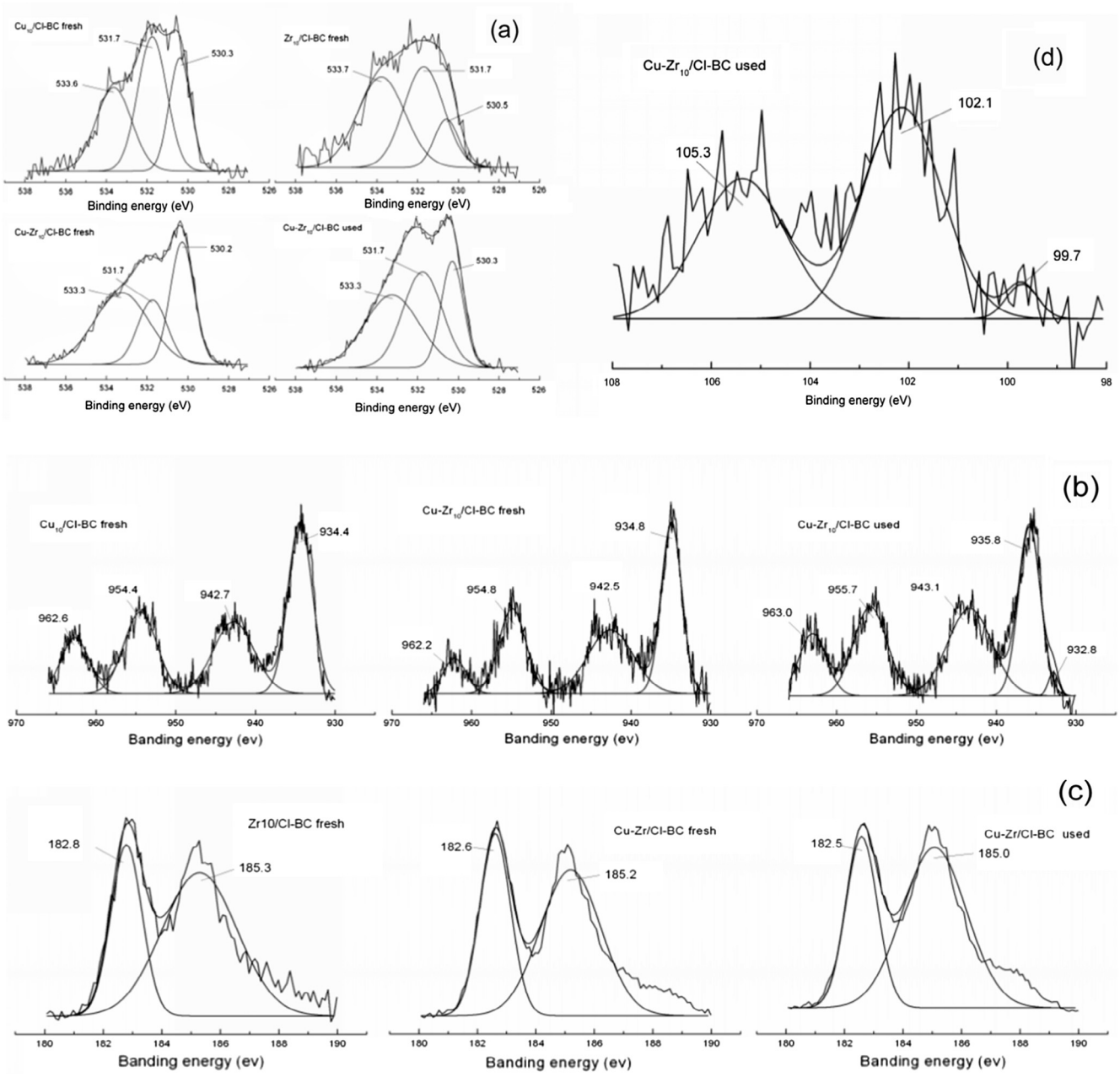

Fig. 8. XPS profiles for fresh Cu_6/Cl-BC, fresh Zr_6/Cl-BC, fresh and used Cu-Zr_{10}/Cl-BC, (a) O 1s (b) Cu 2p (c) Zr 3d (d) Hg 4f.

942.1–943.1 eV and the Cu $2p_{1/2}$ band at 954.4–963.0 eV were three main characteristics of Cu^{2+}. Besides, the absence of the shake-up peak was attributed to reduced copper species [39]. There were no Cu^{+} species could be detected on fresh Cu-Zr_{10}/Cl-BC, while the peak at 932.8 eV ascribed to Cu^{+} shown up on used Cu-Zr_{10}/Cl-BC, which indicated that Cu^{2+} had taken part in the Hg^0 removal and generated Cu^{+} species. Fig. 8(c) presents the Zr 3d spectra of fresh Zr_{10}/Cl-BC, Cu-Zr_{10}/Cl-BC and used Cu-Zr_{10}/Cl-BC. Two primary peaks centered at 182.5–182.8 and 185.0–185.3 eV were ascribed to Zr $3d_{5/2}$ and Zr $3d_{3/2}$ respectively, and they were assigned to Zr^{4+}. The binding energy of zirconium had no distinct change between these catalysts, which suggested that zirconium had neglect effect on Hg^0 oxidation directly [40].

The Hg 4f XPS spectrum of used Cu-Zr_{10}/Cl-BC is shown in Fig. 8 (d). As can be seen from the image, an obvious peak centered at 102.1 eV could be attributed to Si 2p of SiO_2 in quartz wool [41]. The another relative primary peak at 105.3 eV corresponded to Hg $4f_{5/2}$ was assigned to HgO [42], and the small peak at 99.7 eV was ascribed to Hg^0 [43]. This indicated that the main mercury species on the surface of used Cu-Zr10/Cl-BC was HgO. It could be deduced that one mechanism of the Hg^0 removal process followed the step blow, Hg^0 was adsorbed on the surface of the catalysts first, then converted to HgO by reactive surface oxidants [44]. A part of formed HgO (ad) released to flue gases became HgO (g) which determined the oxidation efficiency.

3.5.6. FT-IR

To further investigate the effect of flue gas components during Hg^0 removal reactions, the FT-IR measurements of Cu-Zr_{10}/Cl-BC under SO_2, NH_3, NO and NH_3, H_2O were conducted, and the results are shown in Fig. 9. The spectrum of SO_2 and O_2 adsorption is presented in (a), the band at 925, 1045 cm^{-1} could be assigned to the stretching motion of surface-coordinated sulfite and/or bisulfite [45]. According to some researches, the sulfate could improve the acidity of the catalysts and provide sites especially the Lewis acid sites for NH_3 adsorption, which would facilitate the NH_4^{+} formation and weaken the inhibition of SO_2

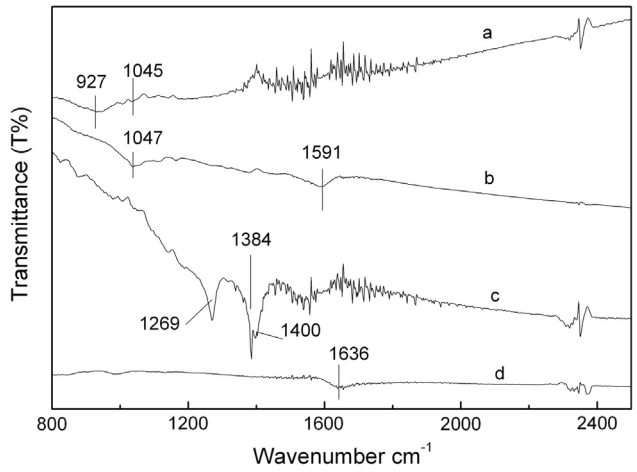

Fig. 9. FTIR spectra over Cu-Zr_{10}/Cl-BC catalyst. Reaction condition: 90 ug/m^3 Hg^0, 6% O_2, N_2 as balance, (a) 400 ppm SO_2 (b) 500 ppm NH_3 (c) NH_3 = NO = 500 ppm (d) 8 vol % H_2O.

[46,47]. The spectra of NH_3 + O_2 adsorption is shown in (b), the bands at 1047, 1590 cm^{-1} were attributed to coordinated NH_3 on Lewis acid sites [48,49]. The spectra after the coadsorption of NH_3, NO and O_2 is presented in (c), two feature bands at 1269 cm^{-1} and 1384 cm^{-1} were corresponded to bridged nitrate and NO_3^- [50], the third band at 1400 cm^{-1} was assigned to ammonium ions (NH_4^+) on Brønsted acid site [19]. It indicated that NH_3 was stably adsorbed on Lewis acid sites and Brønsted acid sites. Besides, the adsorption spectrum of H_2O and O_2 is exhibited in (d), the band at 1636 cm^{-1} could be attributed to δ_{HOH} of H_2O, suggesting that surface water was formed [51].

3.6. Mechanism discussion

From above studies and according to some researches, the possible reaction mechanisms of Hg^0 removal over Cu-Zr_{10}/Cl-BC catalyst were discussed. According to the analysis of XPS Hg 4f, it could be proposed that gas-phase Hg^0 (Hg^0 (g)) was adsorbed on the surface of catalyst to form adsorbed Hg^0 (Hg^0 (ad)) (Eq. (4)). On the one hand, depending on the deduction of SEM-EDX analysis, the activation of Cl^- brought the better texture properties on Cu-Zr_{10}/Cl-BC which enhanced the adsorption ability of Hg^0. The Cl from NH_4Cl could react with C to formed the C-Cl groups [15], and Hg^0 will be captured by C-Cl groups followed Eqs. (5) and (6) [52]. On the other hand, the results of XPS O 1s indicated that the lattice oxygen ([O]) participated in Hg^0 removal process. The adsorbed Hg^0 (Hg^0 (ad)) would be oxidized by [O]. At the same time, the Cu occupied two oxidation states [CuO (Cu^{2+}) ↔ Cu_2O (Cu^+)] during the reaction according to XPS Cu 2p. With the effect of CuO, the consumed [O] would be replenished followed Eq. (7). Zr 3d spectra showed that there existed no distinct valence state change on zirconium, which suggested that ZrO_2 didn't take part in Hg^0 oxidation directly. But the CuO-ZrO_2 interaction made the active components well dispersed on the surface of Cu-Zr_{10}/Cl-BC, which in favor of the catalytic performance. All O element during the reaction came from supplement of O_2 (g), and a part of formed HgO (ad) would desorb from the surface of sample and convert to gas-phase HgO (HgO (g)).

Besides, there might exist the third reaction line according to the results of XRD. The formation of $Cu_2Cl(OH)_3$ appeared on the catalysts loading with CuO and ZrO_2. Its distribution regularities could be deduced that $Cu_2Cl(OH)_3$ might take part in the reaction. $Cu_2Cl(OH)_3$ was first decomposed to Cl-Cu-OH and $Cu(OH)_2$ (detected by XRD), and then Cl-Cu-OH could react with Hg^0 followed Eqs. (11)–(15) [53]. All reaction equations were as follows:

$$Hg^0_{(g)} \rightarrow Hg^0_{(ad)} \quad (4)$$

$$2Cl^- + C{-}C \rightarrow 2C{-}Cl \quad (5)$$

$$Hg^0_{(ad)} + 2C{-}Cl \rightarrow HgCl_{2(ad)} \quad (6)$$

$$2CuO \rightarrow Cu_2O + [O] \quad (7)$$

$$Hg^0(ad) + [O] \rightarrow HgO(ad) \quad (8)$$

$$HgO(ad) \rightarrow HgO(g) \quad (9)$$

$$Cu_2\ O + 1/2O_2 \rightarrow 2CuO \quad (10)$$

$$2ZrOCl_2 + 3H_2O \xrightarrow{\Delta} (ZrO_2)_2 \cdot H_2O + 4HCl \quad (11)$$

$$H{-}OH \rightarrow -OH + H^+ \quad (12)$$

$$Cu^{2+} + Cl^- + 3OH \rightarrow Cu_2Cl(OH)_3 \quad (13)$$

$$Cu_2Cl(OH)_3 \rightarrow Cu(OH)_2 + Cl{-}Cu{-}OH \quad (14)$$

$$4Cl{-}Cu{-}OH + 2Hg^0_{(ad)} + O_2 \rightarrow 4CuO + 2HgCl_2 + 2H_2O \quad (15)$$

3.7. Conclusion

Cu-Zr_x/Cl-BC catalysts were characterized by SEM, BET, XRD, XPS, H_2-TPR and FT-IR. Results suggested that Cu-Zr_{10}/Cl-BC possessed excellent E_T in a broad temperature range, and achieved the best removal efficiency (98.87%) at 120 °C. The gas-phase O_2 had great benefit on Hg^0 removal process especially at high temperature because it could regenerate the lattice oxygen which participated in the removal reaction. Particularly, Hg^0 removal was mainly determined by the adsorption at low temperature and depended on both adsorption and oxidation at high temperature. The catalyst also exhibited well SO_2 and H_2O resistance due to the formation of bidentate sulfates and possessed stable removal activity during the reaction time, which was in favor of the practical application. In addition, the characterization results indicated that Cu-Zr_{10}/Cl-BC catalyst showed lower crystallinity, better texture properties, stronger redox ability with the highly dispersed CuO because of the interaction between CuO and ZrO_2. The mechanism of the Hg^0 removal over Cu-Zr_{10}/Cl-BC was proposed, the effect of Cl^- and the redox shift between Cu^{2+} and Cu^+ were the two main reaction factors responsible for the enhancement of activity. Besides, the exist of $Cu_2Cl(OH)_3$ might also work during the reaction. In conclusion, Cu-Zr_{10}/Cl-BC should be a promising catalyst for Hg^0 removal in flue gas.

Acknowledgements

This work was financially supported by the National Nature Science Foundation of China (51478173), the National Key Research and Development Program of China (2016YFC0204100), and the Scientific and Technological Major Special Project of Hunan Province in China (2015SK1003).

Appendix A. Supplementary data

Supplementary data associated with this article can be found, in the online version, at http://dx.doi.org/10.1016/j.fuel.2018.01.051.

References

[1] Schofield K. Mercury emission control from coal combustion systems: a modified air preheater solution. Combust Flame 2012;159(4):1741–7.
[2] Wang L, et al. Source apportionment of atmospheric mercury pollution in China using the GEOS-Chem model. Environ Pollut 2014;190:166–75.
[3] Yuan Y, et al. Simultaneous removal of SO_2, NO and mercury using TiO_2-aluminum silicate fiber by photocatalysis. Chem Eng J 2012;192:21–8.
[4] Tao S, et al. Activated coke impregnated with cerium chloride used for elemental mercury removal from simulated flue gas. Chem Eng J 2012;210:547–56.
[5] Shen B, et al. Elemental mercury removal by the modified bio-char from waste tea. Fuel 2017;187:189–96.
[6] Wang Lidong, et al. Inhibiting mercury re-emission and enhancing magnesia

recovery by cobalt-loaded carbon nanotubes in a novel magnesia desulfurization process. Environ Sci Technol 2017;51(19):11346–53.
[7] Sjostrom S, et al. Activated carbon injection for mercury control: overview. Fuel 2010;89(6):1320–2.
[8] Mei Z, et al. Removal and recovery of gas-phase element mercury by metal oxide-loaded activated carbon. J Hazard Mater 2008;152(2):721–9.
[9] Zheng Y, et al. Dynamic measurement of mercury adsorption and oxidation on activated carbon in simulated cement kiln flue gas. Fuel 2012;93:649–57.
[10] Granite EJ, et al. The thief process for mercury removal from flue gas. J Environ Manage 2007;84(4):628–34.
[11] Li G, et al. Mechanism identification of temperature influence on mercury adsorption capacity of different halides modified bio-chars. Chem Eng J 2017;315:251–61.
[12] Wang Q, et al. The pyrolysis of biomass briquettes: effect of pyrolysis temperature and phosphorus additives on the quality and combustion of bio-char briquettes. Fuel 2017;199:488–96.
[13] Liu J, et al. Structure sensitivity of selective catalytic reduction of NO with propylene over Cu-doped $Ti_{0.5}Zr_{0.5}O_2-\delta$ catalysts. Appl Catal B 2015;165:519–28.
[14] Hsi H-C, et al. Development of low-concentration mercury adsorbents from bio-hydrogen-generation agricultural residues using sulfur impregnation. Bioresour Technol 2011;102(16):7470–7.
[15] Li G, et al. Elemental mercury removal using biochar pyrolyzed from municipal solid waste. Fuel Process Technol 2015;133:43–50.
[16] Tan Z, et al. Gas-phase elemental mercury removal by novel carbon-based sorbents. Carbon 2012;50(2):362–71.
[17] Bisson TM, et al. Impact of sulfur loading on brominated biomass ash on mercury capture. Energy Fuels 2015;29(12):8110–7.
[18] Rahmaninejad F, Gavaskar VS, Abbasian J. Dry regenerable CuO/γ-Al_2O_3 catalyst for simultaneous removal of SOx and NOx from flue gas. Appl Catal B 2012;119–120:297–303.
[19] Wang T, et al. The catalytic performance and characterization of ZrO_2 support modification on CuO-CeO_2/TiO_2 catalyst for the simultaneous removal of Hg^0 and NO. Appl Surf Sci 2017;400:227–37.
[20] Xu W, et al. CuO/TiO_2 catalysts for gas-phase Hg^0 catalytic oxidation. Chem Eng J 2014;243:380–5.
[21] Wang P, et al. Catalytic oxidation of Hg^0 by CuO–MnO_2–Fe_2O_3/γ-Al_2O_3 catalyst. Chem Eng J 2013;225:68–75.
[22] Guo R-T, et al. Effect of Cu doping on the SCR activity of CeO_2 catalyst prepared by citric acid method. J Ind Eng Chem 2014;20(4):1577–80.
[23] Shi A, et al. The effect of zirconia additive on the activity and structure stability of V_2O_5/WO_3-TiO_2 ammonia SCR catalysis. Appl Catal B 2011;106:359–69.
[24] Li Z, et al. Synergetic catalytic removal of Hg^0 and NO over CeO_2(ZrO_2)/TiO_2. Catal Commun 2016;82:55–60.
[25] Xie J, et al. Novel regenerable sorbent based on Zr–Mn binary metal oxides for flue gas mercury retention and recovery. J Hazard Mater 2013;261:206–13.
[26] Shen B, et al. Elemental mercury removal by the modified bio-char from medicinal residues. Chem Eng J 2015;272:28–37.
[27] He C, et al. Adsorption and oxidation of elemental mercury over Ce-MnOx/Ti-PILCs. Environ Sci Technol 2014;48(14):7891–8.
[28] He C, Shen B, Li F. Effects of flue gas components on removal of elemental mercury over Ce–MnO x/Ti-PILCs. J Hazard Mater 2016;304:10–7.
[29] He C, et al. Elemental mercury removal by CeO_2/TiO_2-PILCs under simulated coal-fired flue gas. Chem Eng J 2016;300:1–8.
[30] Chang H, et al. Design Strategies for CeO2–MoO3Catalysts for DeNOx and Hg0 Oxidation in the Presence of HCl: The Significance of the Surface Acid-Base Properties. Environ Sci Technol 2015;49(20):12388–94.
[31] Yang J, et al. Mercury adsorption and oxidation over cobalt oxide loaded magnetospheres catalyst from fly ash in oxyfuel combustion flue gas. Environ Sci Technol 2015;49(13):8210–8.
[32] Li H, et al. Role of flue gas components in mercury oxidation over TiO_2 supported MnOx-CeO_2 mixed-oxide at low temperature. J Hazard Mater 2012;243:117–23.
[33] Sheng J, et al. Efficient removal of HCHO from simulated coal combustion flue gas using CuO-CeO_2 supported on cylindrical activated coke. Fuel 2017;197:397–406.
[34] Zhang G, et al. Influence of the surface oxygenated groups of activated carbon on preparation of a nano Cu/AC catalyst and heterogeneous catalysis in the oxidative carbonylation of methanol. Appl Catal B 2015;179:95–105.
[35] Wang J, et al. Cerium-stabilized Cu-SSZ-13 catalyst for the catalytic removal of NOx by NH_3. Ind Eng Chem Res 2016;55(5):1174–82.
[36] Ning P, et al. Selective catalytic reduction of NO with NH_3 over CeO_2–ZrO_2–WO_3 catalysts prepared by different methods. Appl Surf Sci 2015;332:130–7.
[37] Liu L, et al. Influence of supports structure on the activity and adsorption behavior of copper-based catalysts for NO reduction. J Mol Catal A: Chem 2010;327(1–2):1–11.
[38] Zhao L, et al. Simultaneous removal of elemental mercury and NO in simulated flue gas over V_2O_5/ZrO_2-CeO_2 catalyst. Appl Catal B 2016;198:420–30.
[39] Peng P-Y, et al. Facile preparation of hierarchical CuO–CeO_2/Ni metal foam composite for preferential oxidation of CO in hydrogen-rich gas. Chem Eng J 2014;251:228–35.
[40] Zhou Z, et al. Manganese doped CeO_2 -ZrO_2 catalyst for elemental mercury oxidation at low temperature. Fuel Process Technol 2016;152:285–93.
[41] Xie Y, et al. Experimental study on Hg^0 removal from flue gas over columnar MnOx-CeO_2/activated coke. Appl Surf Sci 2015;333:59–67.
[42] Xie J, et al. Synthesis and characterization of nano-sized Mn–TiO_2 catalysts and their application to removal of gaseous elemental mercury. Res Chem Intermed 2012;38(9):2511–22.
[43] Zhang X, et al. Simultaneous removal of elemental mercury and NO from flue gas by V_2O_5–CeO_2/TiO_2 catalysts. Appl Surf Sci 2015;347:392–400.
[44] Lee Woojin, et al. Removal of elemental mercury (Hg(0)) by nannosized V2O5/TiO2 catalysts. Environ Sci Technol 2009;43:1522–7.
[45] Zhao L, et al. SO_2 adsorption and transformation on calcined NiAl hydrotalcite-like compounds surfaces: An in situ FTIR and DFT study. Appl Catal B 2012;117–118:339–45.
[46] Jiang BQ, et al. Drift study of the SO_2 effect on low-temperature SCR reaction over Fe-Mn/TiO_2. Chem C 2010;114:4961–5.
[47] Chang H, et al. Effect of Sn on MnOx–CeO_2 catalyst for SCR of NOx by ammonia: enhancement of activity and remarkable resistance to SO_2. Catal Commun 2012;27:54–7.
[48] Cao F, et al. The activity and characterization of MnOx–CeO_2–ZrO_2/γ-Al_2O_3 catalysts for low temperature selective catalytic reduction of NO with NH_3. Chem Eng J 2014;243:347–54.
[49] Wang J, et al. In situ DRIFTS investigation on the SCR of NO with NH_3 over V_2O_5 catalyst supported by activated semi-coke. Appl Surf Sci 2014;313:660–9.
[50] Zhang J, et al. A sol-gel Ti-Al-Ce-nanoparticle catalyst for simultaneous removal of NO and Hg^0 from simulated flue gas. Chem Eng J 2017;313:1535–47.
[51] Chen W, et al. Mechanism of the Selective Catalytic Oxidation of Slip Ammonia over Ru-Modified Ce–Zr Complexes Determined by in Situ Diffuse Reflectance Infrared Fourier Transform Spectroscopy. Environ Sci Technol 2014;48(20):12199–205.
[52] Li G, et al. Removal of element mercury by medicine residue derived biochars in presence of various gas compositions. J Hazard Mater 2015;298:162–9.
[53] Zhou X, et al. The enhance effect of atomic Cl in $CuCl_2$/TiO_2 catalyst for Hg^0 catalytic oxidation. Chem Eng J 2014;254:82–7.